Received: 30 December 2021 | Accepted: 20 June 2022

DOI: 10.1002/nme.7061

RESEARCH ARTICLE

WILEY

Local knot method for solving inverse Cauchy problems of Helmholtz equations on complicated two- and three-dimensional domains

Fajie Wang[1,2] | **Zengtao Chen**[1] | **Yanpeng Gong**[3]

[1]National Engineering Research Center for Intelligent Electrical Vehicle Power System, College of Mechanical and Electrical Engineering, Qingdao University, Qingdao, China

[2]Institute of Mechanics for Multifunctional Materials and Structures, Qingdao University, Qingdao, China

[3]Institute of Electronics Packaging Technology and Reliability, Faculty of Materials and Manufacturing, Beijing University of Technology, Beijing, China

Correspondence
Fajie Wang, National Engineering Research Center for Intelligent Electrical Vehicle Power System, College of Mechanical and Electrical Engineering, Qingdao University, Qingdao 266071, China.
Email: wfj1218@126.com
Yanpeng Gong, Institute of Electronics Packaging Technology and Reliability, Faculty of Materials and Manufacturing, Beijing University of Technology, Beijing 100124, China.
Email: yanpeng.gong@bjut.edu.cn

Funding information
National Natural Science Foundation of China, Grant/Award Number: 11802151; Natural Science Foundation of Shandong Province, Grant/Award Number: ZR2019BA008

Abstract

This article presents a local knot method (LKM) to solve inverse Cauchy problems of Helmholtz equations in arbitrary 2D and 3D domains. The Moore–Penrose pseudoinverse using the truncated singular value decomposition is employed in the local approximation of supporting domain instead of the moving least squares method. The developed approach is a semi-analytical and local radial basis function collocation method using the non-singular general solution as the basis function. Like the traditional boundary knot method, the LKM is simple, accurate and easy-to-program in solving inverse Cauchy problems associated with Helmholtz equations. Unlike the boundary knot method, the new scheme can directly reconstruct the unknowns both inside the physical domain and along its boundary by solving a sparse linear system, and can achieve a satisfactory solution. Numerical experiments, involving the complicated geometry and the high noise level, confirm the accuracy and reliability of the proposed method for solving inverse Cauchy problems of Helmholtz equations.

KEYWORDS

Helmholtz equations, inverse Cauchy problems, local knot method, Moore–Penrose pseudoinverse, non-singular general solution

1 | INTRODUCTION

The Helmholtz equations arise in various applications of science and engineering, such as acoustics, electromagnetic scattering, and heat conduction in nuclear reactors. In general, boundary conditions on the complete boundary are provided in the numerical computation. This is the so-called forward problem, which is well-posed and is relatively easy to solve. Up to now, various numerical methods have been proposed for solving such problems, such as the method of fundamental solutions,[1,2] the boundary element method,[3] and coupling with other methods.[4,5] In many real-world problems,

however, a part of boundary conditions cannot be specified due to the difficulty in measurement.[6] To address this problem effectively, additional data must be obtained from the measurable or accessible boundary. With this regard, an over-determined problem will need to be addressed to determine the boundary conditions on the unspecified part of boundary, and to approximate the unknowns inside the computational domain. This is called the inverse Cauchy problem,[7–10] which is usually ill-conditioned in the sense that a small perturbation in the boundary data may result in enormous deviation in the solution.

In the numerical simulation of the inverse Cauchy problems, boundary-type methods are widely used due to their merits in the reconstruction of boundary data. Marin et al.[11,12] proposed the method of fundamental solutions for the Cauchy problem associated with Helmholtz-type equations. Chen et al.[13] used the boundary particle method for solving inverse Cauchy problems of inhomogeneous Helmholtz equations. Fan et al.[14] proposed a local radial basis function collocation method for solving two-dimensional inverse Cauchy problem. Liu et al.[15] introduced a novel Trefftz method to solve the inverse Cauchy problem of 3D modified Helmholtz equation. Jin et al.[16,17] employed the boundary knot method (BKM) to solve the Cauchy problem associated with the Helmholtz equation, and their main work focuses on the 2D cases. The BKM is boundary-type radial basis function method using the non-singular general solution as the basis function, and has the merits of simplicity, accuracy, and meshless. However, its matrices are usually ill-conditioned,[18,19] and the appropriate regularization techniques have to be introduced in solving the resultant system.[16,17] Furthermore, as a boundary-type meshless scheme with global discretization, the BKM encounters the challenge of simulating large-scale and/or high-dimensional problems.

Recently, the localized boundary knot method (LBKM)[20,21] has been proposed to overcome above shortcomings. The LBKM is a domain-type meshfree approach using the non-singular general solution as the basis function. In fact, it can be regarded as a localized version of traditional boundary-type BKM. When this method was first proposed, the artificial boundaries and boundary nodes on it are required for every local subdomain. Latter, the LBKM is modified into the local knot method (LKM)[22,23] without designing the artificial boundaries, which likes a local radial basis function collocation method. Consequently, the calculation process is simplified, and the calculation efficiency is improved with the same calculation accuracy. Recently, the LKM has been used to simulate acoustics and convection-diffusion problems, and has demonstrated the advantages of truly meshless, high-accuracy, and large-scale calculation.

In recent years, the local semi-analytical meshless collocation methods, such as the localized method of fundamental solutions (LMFS),[24,25] localized singular boundary method (LSBM)[26] and LKM, have attracted more and more attention due to their high-accuracy and meshless. This kind of method adopts semi-analytical basis functions satisfied governing equations to approximate the solution of partial differential equation. The LMFS and LSBM use the singular fundamental solution, while the LKM uses the non-singular general solution. To deal with the singularity, the first two methods respectively introduce the fictitious boundary and the origin intensity factor, which is troublesome and has a certain impact on the calculation accuracy. However, the latter approach does not require the additional operating procedure thanks to the use of non-singular basis functions. In conclusion, the LKM is more stable and easy-to-program compared with the LMFS and LSBM. At present, this method only focuses on the numerical simulation of the forward problem. It should be pointed out that the solution of the inverse problem is much more difficult than the forward problem due to the absence of boundary conditions.

In this article, we propose a novel numerical method to solve inverse Cauchy problems of Helmholtz equations on complicated two- and three-dimensional domains, by combining the LKM the Moore–Penrose pseudoinverse technique. It is not an easy work to solve acoustic inverse problems related to high-dimensional complex geometries by using the traditional finite element and finite difference methods for a long time. The main novelty of this article lies in that we established a simple, accurate, and stable numerical framework for addressing the inverse Cauchy problems of Helmholtz equations on arbitrarily complicated domains. The Moore–Penrose pseudoinverse in the local approximation employs the truncated singular value decomposition to eliminate the ill-condition of the local system, so that a well-conditioned system of sparse equations can be generated. Compared with the traditional boundary-type BKM in which regularization techniques have to be used in solving the resultant system, the present scheme can greatly reduce the computational expense. Moreover, the unknowns both inside the physical domain and along its boundary can be directly and accurately reconstructed by solving a sparse linear system.

The organization of this article is as follows. Section 2 briefly reviews the inverse Cauchy problems of Helmholtz equations. In Section 3, the numerical procedures of proposed LKM are described for dealing with the inverse Cauchy problems of Helmholtz equations on two- and three-dimensional domains. Section 4 introduces two local approximation techniques (the Moore–Penrose pseudoinverse and the moving least-squares (MLS)) of supporting domain in the LKM. Followed by Section 5 presents four examples to illustrate

the validity and accuracy of the proposed methodology. Finally, some conclusions and remarks are drawn in Section 6.

2 | MATHEMATICAL PRELIMINARIES

The inverse Cauchy problem of Helmholtz-type equation is stated in the following general form:

$$Lu(\boldsymbol{x}) = 0, \quad \boldsymbol{x} \in \Omega \subset \mathbf{R}^d, \tag{1}$$

$$u(\boldsymbol{x}) = f(\boldsymbol{x}) \qquad \text{for } \boldsymbol{x} \in \Gamma_1, \tag{2}$$

$$\frac{\partial u(\boldsymbol{x})}{\partial \boldsymbol{n}} = g(\boldsymbol{x}) \qquad \text{for } \boldsymbol{x} \in \Gamma_1, \tag{3}$$

where $L = \nabla^2 \pm k$ is the Helmholtz-type differential operator (Equation (1) is known as the Helmholtz equation when $L = \nabla^2 + k$, and it is called the modified Helmholtz equation when $L = \nabla^2 - k$), Ω the problem domain whose boundary is $\partial\Omega = \Gamma_1 + \Gamma_2$, d the space dimension, k the wave number, $\boldsymbol{n}$ the unit outward normal vector, $f(\boldsymbol{x})$ and $g(\boldsymbol{x})$ are given functions on the accessible boundary Γ_1. In this model, no boundary condition is available on the rest part of boundary (Γ_2), called the inaccessible boundary. Figure 1 shows a sketch of the inverse Cauchy problems in 2D case. The 3D case is similar, only differing in that the boundary becomes a surface.

The non-singular general solution of Equation (1) can be given by[16,20]

$$G(r) = \begin{cases} J_0(kr), & d = 2, \\ \sin(kr)/r, & d = 3, \end{cases} \qquad \text{for} \quad L = \nabla^2 + k, \tag{4}$$

$$G(r) = \begin{cases} I_0(kr), & d = 2, \\ \sinh(kr)/r, & d = 3, \end{cases} \qquad \text{for} \quad L = \nabla^2 - k, \tag{5}$$

where J_0 and I_0 are the zero-order Bessel function of the first kind and the zero-order modified Bessel function of the first kind, respectively.

The solution of the above inverse problem usually requires the reconstruction of sound field on the inaccessible boundary and inside the physical domain, based on the known information on the accessible boundary. Unlike the direct problem, the inverse problem has always been a difficult issue in computational mathematics and mechanics, especially for 3D complex geometries. Most of the existing methods need regularization techniques when solving the final system of algebraic equations, and are troublesome and time-consuming. This article will introduce a novel LKM to address such problems in the next section.

3 | LOCAL KNOT METHOD FOR INVERSE CAUCHY PROBLEM OF HELMHOLTZ EQUATION

First of all, $N = n_i + n_{b1} + n_{b2}$ discrete nodes $\boldsymbol{x}^{(i)}$, $i = 1, 2, \ldots, N$ are placed over the computational domain Ω, where N is the number of nodes inside the domain, n_{b1} and n_{b2} indicate the numbers of nodes along the accessible and inaccessible

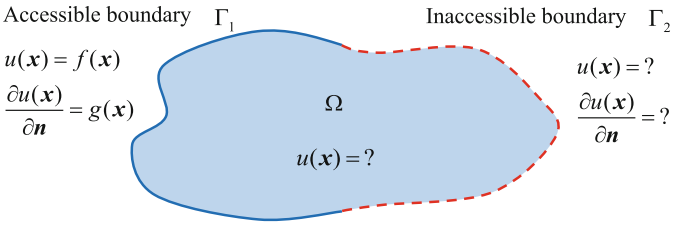

FIGURE 1 Sketch of the inverse Cauchy problems in 2D case

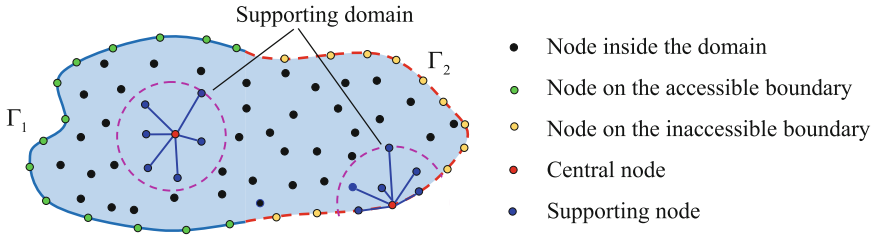

FIGURE 2 Schematic diagram of the LKM for inverse Cauchy problems of 2D Helmholtz equations

boundary, respectively. Considering an arbitrary node $\boldsymbol{x}^{(i)}$ called as the central node, its m supporting nodes $\boldsymbol{x}_j^{(i)}$, $j = 1, 2, \dots, m$ can be determined from nearest nodes. Figure 2 shows the schematic diagram of the LKM for 2D problem, the 3D problem has the same principle.

Using $\boldsymbol{x}_0^{(i)}$ to represent $\boldsymbol{x}^{(i)}$, the unknowns at nodes $\boldsymbol{x}_j^{(i)}$, $j = 0, 1, \dots, m$ are expressed as

$$u\left(\boldsymbol{x}_j^{(i)}\right) = \sum_{k=0}^{m} \alpha_k^{(i)} G\left(r_{jk}\right), \quad j = 0, 1, \dots, m, \tag{6}$$

where $r_{jk} = \left\|\boldsymbol{x}_k^{(i)} - \boldsymbol{x}_j^{(i)}\right\|_2$, and $\boldsymbol{\alpha}^{(i)} = \left[\alpha_0^{(i)}, \alpha_1^{(i)}, \alpha_2^{(i)}, \dots, \alpha_m^{(i)}\right]^{\mathrm{T}}$ are the unknown coefficients. Equation (6) can be rewritten in the following matrix form:

$$\boldsymbol{u}^{(i)} = \boldsymbol{G}^{(i)} \boldsymbol{\alpha}^{(i)}. \tag{7}$$

In general, $\boldsymbol{\alpha}^{(i)}$ can be calculated by solving Equation (7) in the BKM. However, $\boldsymbol{u}^{(i)}$ is unknown in the LKM, and thus is used to express $\boldsymbol{\alpha}^{(i)}$,

$$\boldsymbol{\alpha}^{(i)} = \boldsymbol{H}^{(i)} \boldsymbol{u}^{(i)}, \tag{8}$$

where $\boldsymbol{H}^{(i)}$ is a matrix of order $(m+1) \times (m+1)$. It is noticed that the matrix $\boldsymbol{G}^{(i)}$ usually has a large condition number, due to the properties of nonsingular general solutions. Therefore, a proper approach should be adopted to approximate the unknown coefficient vector $\boldsymbol{\alpha}^{(i)}$ in the supporting domain. Two simple and effective methods will be discussed in the next section.

Replacing $\boldsymbol{x}_j^{(i)}$ in Equation (6) with $\boldsymbol{x}^{(i)}$, the following formula is yielded

$$u\left(\boldsymbol{x}^{(i)}\right) = \sum_{k=0}^{m} \alpha_k^{(i)} G\left(r_{0k}\right) = \boldsymbol{C}^{(i)} \boldsymbol{\alpha}^{(i)}, \tag{9}$$

and then substituting Equation (8) into Equation (9), we have

$$u\left(\boldsymbol{x}^{(i)}\right) = \boldsymbol{C}^{(i)} \boldsymbol{H}^{(i)} \boldsymbol{u}^{(i)} = \boldsymbol{D}^{(i)} \boldsymbol{u}^{(i)}. \tag{10}$$

If $\boldsymbol{x}^{(i)}$ is a node on the boundary, the normal derivative can be calculated by

$$\frac{\partial u\left(\boldsymbol{x}^{(i)}\right)}{\partial \boldsymbol{n}} = \boldsymbol{N}^{(i)} \boldsymbol{\alpha}^{(i)} = \boldsymbol{N}^{(i)} \boldsymbol{H}^{(i)} \boldsymbol{u}^{(i)} = \boldsymbol{E}^{(i)} \boldsymbol{u}^{(i)}, \tag{11}$$

where

$$\begin{cases} \boldsymbol{N}^{(i)} = n_1 \boldsymbol{\sigma}_1^{(i)} + \cdots + n_d \boldsymbol{\sigma}_d^{(i)}, \\ \boldsymbol{\sigma}_l^{(i)} = \left[\frac{G(r_{i0})}{\partial x_l^{(i)}}, \frac{G(r_{i1})}{\partial x_l^{(i)}}, \dots, \frac{G(r_{im})}{\partial x_l^{(i)}}\right], \quad l = 1, \dots, d. \end{cases} \tag{12}$$

In above equations, $n_1, \ldots, n_d$ denote the components of the vector $\boldsymbol{n}$, and $x_1^{(i)}, \ldots, x_d^{(i)}$ denote the coordinate components of the node $\boldsymbol{x}^{(i)}$.

Taking into account all the nodes $\boldsymbol{x}^{(i)}$, $i = 1, 2, \ldots, N$ and boundary data given in Equations (2) and (3), the following overdetermined equations can be obtained,

$$\begin{cases} u_i - \boldsymbol{D}^{(i)}\boldsymbol{u}^{(i)} = 0, \quad i \in \{1, 2, \ldots, n_i\} \cup \{n_i + n_{b1} + 1, \ldots, N\} \\ u_i = f_i, \quad i \in \{n_i + 1, \ldots, n_i + n_{b1}\} \\ \boldsymbol{E}^{(i)}\boldsymbol{u}^{(i)} = g_i, \quad i \in \{n_i + 1, \ldots, n_i + n_{b1}\} \end{cases} \quad \text{or} \quad \boldsymbol{A}\boldsymbol{u} = \boldsymbol{b}, \tag{13}$$

where $\boldsymbol{u} = \left[u\left(\boldsymbol{x}^{(1)}\right), \; u\left(\boldsymbol{x}^{(2)}\right), \; \ldots, \; u\left(\boldsymbol{x}^{(N)}\right)\right]^T$, $\boldsymbol{b}_{(N+n_{b1})\times 1}$ is a vector composed of zero elements and boundary data, and $\boldsymbol{A}_{(N+n_{b1})\times N}$ is a sparse matrix. Equation (13) is a well-conditioned system, and is solved by MATLAB routine "$\boldsymbol{A}\backslash\boldsymbol{b}$" in this study.

4 | APPROXIMATION OF UNKNOWN COEFFICIENTS IN THE SUPPORTING DOMAIN

The accurate calculation of the matrix $\boldsymbol{H}^{(i)}$ in Equation (8) plays a crucial role for the accuracy and efficiency of the LKM. This study investigates two commonly used methods: the MLS approximation and the Moore–Penrose pseudoinverse. The following is a brief introduction to these two techniques.

4.1 | The Moore–Penrose pseudoinverse (MPP)

The most straightforward way to obtain the matrix $\boldsymbol{H}^{(i)}$ in Equation (8) is by solving the inverse matrix of $\boldsymbol{G}^{(i)}$. Considering the singularity and ill-condition of the matrix $\boldsymbol{G}^{(i)}$, the Moore–Penrose pseudoinverse $\boldsymbol{H}^{(i)} = \left[\boldsymbol{G}^{(i)}\right]^+$ is used. The Moore–Penrose pseudoinverse[27] is a matrix that can act as a partial replacement for the matrix inverse in cases where it does not exist or cannot solved accurately. The matrix $\left[\boldsymbol{G}^{(i)}\right]^+$ is called the generalized inverse of the matrix $\boldsymbol{G}^{(i)}$, and satisfies the following conditions:

$$\begin{cases} \boldsymbol{G}^{(i)}\left[\boldsymbol{G}^{(i)}\right]^+\boldsymbol{G}^{(i)} = \boldsymbol{G}^{(i)}, \\ \left[\boldsymbol{G}^{(i)}\right]^+\boldsymbol{G}^{(i)}\left[\boldsymbol{G}^{(i)}\right]^+ = \left[\boldsymbol{G}^{(i)}\right]^+, \\ \left(\boldsymbol{G}^{(i)}\left[\boldsymbol{G}^{(i)}\right]^+\right)^* = \boldsymbol{G}^{(i)}\left[\boldsymbol{G}^{(i)}\right]^+, \\ \left(\left[\boldsymbol{G}^{(i)}\right]^+\boldsymbol{G}^{(i)}\right)^* = \left[\boldsymbol{G}^{(i)}\right]^+\boldsymbol{G}^{(i)}. \end{cases} \tag{14}$$

There are many approaches for computing the Moore–Penrose inverse of a matrix. Among them, the truncated singular value decomposition (TSVD) is one of the most frequently used method. This method is the algorithm behind the in-built pseudoinverse computing function "*pinv*(*A*, *tol*)" in MATLAB.[28] Here, *tol* is the singular value tolerance, specified as a scalar. *Pinv* treats singular values that are smaller than *tol* as zeros during the computation of the pseudoinverse.

By using the SVD, $\boldsymbol{G}^{(i)}$ can be decomposed into

$$\boldsymbol{G}^{(i)} = \boldsymbol{U}\boldsymbol{S}\boldsymbol{V}^*, \tag{15}$$

where $\boldsymbol{U}_{(m+1)\times(m+1)}$ and $\boldsymbol{V}_{(m+1)\times(m+1)}$ are the unit orthogonal matrixes, $\boldsymbol{S} = \mathrm{diag}\,(s_1, s_2, \ldots, s_{m+1})$ is a diagonal matrix with non-negative elements in non-increasing order, $\left\{s_j\right\}_{j=1}^{m+1}$ are called the singular values of matrix $\boldsymbol{G}^{(i)}$. Let $s_j = 0$ when $s_j < tol$, Equation (15) can be rewritten as

$$\boldsymbol{G}^{(i)} = \boldsymbol{U}\boldsymbol{S}\boldsymbol{V}^* = [\boldsymbol{U}_1 \;\; \boldsymbol{U}_2]\begin{bmatrix} \boldsymbol{S}_1 & 0 \\ 0 & 0 \end{bmatrix}[\boldsymbol{V}_1 \;\; \boldsymbol{V}_2]^* = \boldsymbol{U}_1\boldsymbol{S}_1\boldsymbol{V}_1^*. \tag{16}$$

Then, the pseudoinverse of $\boldsymbol{G}^{(i)}$ can be calculated by the following formula:

$$\left[\boldsymbol{G}^{(i)}\right]^{+} = \boldsymbol{V}_1 \boldsymbol{S}_1^{-1} \boldsymbol{U}_1^{*}. \tag{17}$$

4.2 | The moving least-squares (MLS)

The MLS approximation is a widely used technique in various meshless/meshfree methods. According to its basic idea, the vector $\boldsymbol{\alpha}^{(i)}$ is deduced by minimizing the following functional,

$$\ell \boldsymbol{u}^{(i)} = \left(\boldsymbol{G}^{(i)}\boldsymbol{\alpha}^{(i)} - \boldsymbol{u}^{(i)}\right)^{\mathrm{T}} \boldsymbol{\omega}^{(i)} \left(\boldsymbol{G}^{(i)}\boldsymbol{\alpha}^{(i)} - \boldsymbol{u}^{(i)}\right), \tag{18}$$

where

$$\begin{cases} \boldsymbol{\omega}^{(i)} = diag\left(w_0^{(i)}, w_1^{(i)}, \ldots, w_m^{(i)}\right), \\ \omega_j^{(i)} = 1 - 6\left(d_j/d_{\max}\right)^2 + 8\left(d_j/d_{\max}\right)^3 - 3\left(d_j/d_{\max}\right)^4, \\ d_j = \left\|\boldsymbol{x}_j^{(i)} - \boldsymbol{x}^{(i)}\right\|_2, \\ d_{\max} = \max\limits_{j=0,1,\ldots,m}\left(d_j\right). \end{cases} \tag{19}$$

Hence, we have

$$\frac{\partial \ell \boldsymbol{u}^{(i)}}{\partial \boldsymbol{\alpha}^{(i)}} = 0. \tag{20}$$

By calculating and reorganizing Equation (20), we can get a system equation in matrix form,

$$\boldsymbol{L}^{(i)}\boldsymbol{\alpha}^{(i)} = \boldsymbol{P}^{(i)}, \tag{21}$$

where

$$\boldsymbol{L}^{(i)} = \begin{bmatrix} \sum\limits_{j=0}^{m}\left[G\left(r_{j0}\right)\right]^2\omega_j^{(i)} & \sum\limits_{j=0}^{m}G\left(r_{j0}\right)G\left(r_{j1}\right)\omega_j^{(i)} & \sum\limits_{j=0}^{m}G\left(r_{j0}\right)G\left(r_{j2}\right)\omega_j^{(i)} & \cdots & \sum\limits_{j=0}^{m}G\left(r_{j0}\right)G\left(r_{jm}\right)\omega_j^{(i)} \\ & \sum\limits_{j=0}^{m}\left[G\left(r_{j1}\right)\right]^2\omega_j^{(i)} & \sum\limits_{j=0}^{m}G\left(r_{j1}\right)G\left(r_{j2}\right)\omega_j^{(i)} & \cdots & \sum\limits_{j=0}^{m}G\left(r_{j1}\right)G\left(r_{jm}\right)\omega_j^{(i)} \\ & & \sum\limits_{j=0}^{m}\left[G\left(r_{j2}\right)\right]^2\omega_j^{(i)} & \cdots & \sum\limits_{j=0}^{m}G\left(r_{j2}\right)G\left(r_{jm}\right)\omega_j^{(i)} \\ & SYM & & \ddots & \vdots \\ & & & & \sum\limits_{j=0}^{m}\left[G\left(r_{jm}\right)\right]^2\omega_j^{(i)} \end{bmatrix}, \tag{22}$$

$$\boldsymbol{P}^{(i)} = \begin{bmatrix} \sum_{j=0}^{m}G\left(r_{j0}\right)\omega_j^{(i)}u\left(\boldsymbol{x}_j^{(i)}\right) \\ \sum_{j=0}^{m}G\left(r_{j1}\right)\omega_j^{(i)}u\left(\boldsymbol{x}_j^{(i)}\right) \\ \sum_{j=0}^{m}G\left(r_{j2}\right)\omega_j^{(i)}u\left(\boldsymbol{x}_j^{(i)}\right) \\ \vdots \\ \sum_{j=0}^{m}G\left(r_{jm}\right)\omega_j^{(i)}u\left(\boldsymbol{x}_j^{(i)}\right) \end{bmatrix} = \begin{bmatrix} G\left(r_{00}\right)\omega_0^{(i)} & G\left(r_{10}\right)\omega_1^{(i)} & \cdots & G\left(r_{m0}\right)\omega_m^{(i)} \\ G\left(r_{01}\right)\omega_0^{(i)} & G\left(r_{11}\right)\omega_1^{(i)} & \cdots & G\left(r_{m1}\right)\omega_m^{(i)} \\ \vdots & \vdots & \ddots & \vdots \\ G\left(r_{0m}\right)\omega_0^{(i)} & G\left(r_{1m}\right)\omega_1^{(i)} & \cdots & G\left(r_{mm}\right)\omega_m^{(i)} \end{bmatrix} \begin{pmatrix} u\left(\boldsymbol{x}_0^{(i)}\right) \\ u\left(\boldsymbol{x}_1^{(i)}\right) \\ \vdots \\ u\left(\boldsymbol{x}_m^{(i)}\right) \end{pmatrix} = \boldsymbol{Q}^{(i)}\boldsymbol{u}^{(i)}. \tag{23}$$

Substituting Equation (23) into Equation (21), we have

$$\boldsymbol{L}^{(i)}\boldsymbol{\alpha}^{(i)} = \boldsymbol{Q}^{(i)}\boldsymbol{u}^{(i)}. \tag{24}$$

Let $\boldsymbol{H}^{(i)} = \left[\boldsymbol{L}^{(i)}\right]^{-1}\boldsymbol{Q}^{(i)}$, then $\boldsymbol{\alpha}^{(i)} = \boldsymbol{H}^{(i)}\boldsymbol{u}^{(i)}$. It should be pointed out that we directly use the MATLAB's mldivide (matrix left divide) function ($\boldsymbol{L}^{(i)}\backslash\boldsymbol{Q}^{(i)}$) to get $\boldsymbol{H}^{(i)}$, instead of the matrix inversion.

5 | NUMERICAL RESULTS AND DISCUSSIONS

In this section, two numerical examples are investigated to verify the performance of the proposed algorithm. The maximum absolute error (*MAE*) and root mean square error (*RMSE*) are calculated as:

$$MAE = \max_{1\le i\le N} \left| u_{\mathrm{a}}\left(\boldsymbol{x}^{(i)}\right) - u_{\mathrm{n}}\left(\boldsymbol{x}^{(i)}\right)\right|, \tag{25}$$

$$RMSE = \left[\frac{1}{N}\sum_{i=1}^{N}\left(u_{\mathrm{a}}\left(\boldsymbol{x}^{(i)}\right) - u_{\mathrm{n}}\left(\boldsymbol{x}^{(i)}\right)\right)^2\right]^{1/2}, \tag{26}$$

where u_{a} and u_{n} denote the analytical and numerical solutions at the node $\boldsymbol{x}^{(i)}$, respectively. The noise with the level δ is imposed in the boundary conditions by

$$f_i = f_i(1 + \delta R), \quad g_i = g_i(1 + \delta R), \tag{27}$$

where R is a random number between $[-1, 1]$. In addition, the percentage of the accessible boundary is assumed as σ, and the rest part is the inaccessible boundary.

Example 1. The first example considers a circular domain $\Omega = \left\{(x_1, x_2)\,|x_1^2 + x_2^2 \le 1\right\}$, and we investigate the following two analytical solutions satisfied Helmholtz equation with $k = \sqrt{2}$ and $k = 1$:

$$\text{Solution I}: u(x_1, x_2) = \sin(x_1)\sin(x_2), \tag{28}$$

$$\text{Solution II}: u(x_1, x_2) = \sin\left(\sqrt{2}x_1\right)\sinh(x_2) + \cos(x_2). \tag{29}$$

First, the accessible and inaccessible boundaries are assumed to be $\Gamma_1 = \{(R, \theta) \mid 0 \le \theta < 3\pi/2,\ \ R = 1\}$ and $\Gamma_2 = \{(R, \theta)|3\pi/2 \le \theta < 2\pi,\ \ R = 1\}$, respectively. In other word, the percentage of the accessible boundary is $\sigma = 75\%$. To numerically solve this problem, $N = 2118$ total nodes including 200 uniformly distributed boundary nodes are chosen, and $m = 30$ supporting nodes are fixed. Adding 2% noise to the boundary data, Figure 3 shows the comparisons of analytical solution and LKM solutions on the inaccessible boundary for the solutions I and II. In the present calculation, the LKM uses the different local approximation techniques (MLS and MPP). The MLS adopted the quartic spline function, exponential function and Gaussian function as the weighting functions, and the MPP set the singular value tolerance to 1e-03, 1e-04, 1e-05, and 1e-06. We can see from Figure 3 that the results from the MPPs with *tol* = 1e-05 and *tol* = 1e-06 are overlapped absolutely, and have the highest accuracy compared to other local approximation techniques.

Next, we set $\delta = 3\%$ with other parameters constant. Table 1 lists the MAEs and RMSEs obtained by the LKM with various techniques of local approximation. Noted that the errors from the MPPs with *tol* = 1e-05 and *tol* = 1e-06 are exactly the same for two different solutions. On the whole, the MPPs with *tol* = 1e-05 and *tol* = 1e-06 have better accuracy and stability compared to other local approximation techniques. For the sake of simplicity, the MPP with *tol* = 1e-05 will be adopted in the following calculations unless otherwise specified.

To investigate the influence of the noise level and the percentage of the accessible boundary on the numerical accuracy, Figure 4 plots the error curves of the LKM under the different values of δ and σ, where $N = 2118$ and $m = 30$. σ is taken to be 75% in the first test (Figure 4A), and δ is taken to be 3% in the second test (Figure 4B). As expected, the error gradually decreases with the decreasing noise level as well as the increasing percentage of the accessible boundary, indicating the good convergence of the proposed approach.

Finally, Table 2 gives the MAEs, RMSEs, CPU-times under different numbers of supporting node, where solution I is tested, $\delta = 3\%$ and $\sigma = 75\%$ are chosen. As can be seen, the proposed scheme is accurate and stable. The errors remain roughly constant for various values of m. Moreover, more CPU-time is consumed as the number (m) increases. Comprehensively speaking, the relatively few supporting nodes ($20 \le m \le 40$) can achieve satisfactory accuracy.

Example 2. A Helmholtz equation on a piecewise smooth domain (see Figure 5A) is considered in this example.[16] The boundary is divided into two disjointed parts, the accessible part Γ_1 and the inaccessible part Γ_2. For the convenience of comparison and illustration of the accuracy of the method, the following analytical solution with $k = 1$ is investigated,

$$u(x_1, x_2) = x_1 \sin(x_2). \tag{30}$$

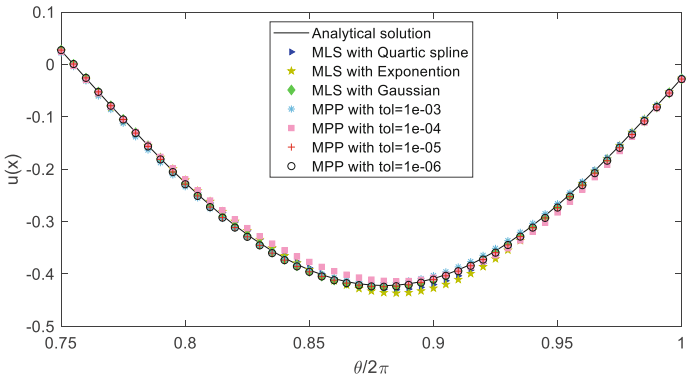

(A)

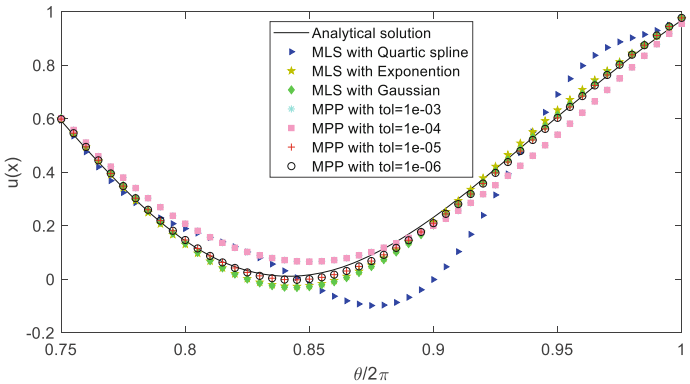

(B)

FIGURE 3 Comparison of analytical solution and LKM solutions on the inaccessible boundary for (A) solution I and (B) solution II, under $\delta = 2\%$ and $\sigma = 75\%$. The LKM used the MLS and the MPP for the local approximation of supporting domain, the MLS adopted three different types of weighting function, and the MPP used four different values of the singular value tolerance.

TABLE 1 The MAEs and RMSEs obtained by the LKM with various techniques of local approximation, under $\delta = 3\%$ and $\sigma = 75\%$

Local approximation techniques	Solution I		Solution II	
	MAE	RMSE	MAE	RMSE
MLS with Quartic spline	1.158e-02	3.403e-03	2.384e-01	2.891e-02
MLS with Exponention	1.869e-02	3.238e-03	4.113e-02	1.099e-02
MLS with Gaussian	7.833e-03	1.980e-03	4.556e-02	1.130e-02
MPP with tol = 1e-03	8.507e-03	3.625e-03	7.097e-02	1.615e-02
MPP with tol = 1e-04	1.518e-02	3.406e-03	7.097e-02	1.615e-02
MPP with tol = 1e-05	8.124e-03	2.078e-03	2.729e-02	1.010e-02
MPP with tol = 1e-06	8.124e-03	2.078e-03	2.729e-02	1.010e-02

As shown in Figure 5B, $N = 659$ total nodes including 138 boundary nodes are chosen over the computational domain. When the number of supporting nodes is set to $m = 30$, Figure 6 illustrates the reconstructed results on the inaccessible boundary under various noise levels. It is observed from Figure 6 that the predicted results converge to the analytical solution as the amount of noise in the data decreases. Even for a relatively high amount of noise (3%) added into the data, the numerical results still agree well with the analytical solutions. In addition, Figure 7 displays the numerical and analytical solutions on the computational domain with 2% noise level. Noted that the predicted result coincide with the analytical one quite well.

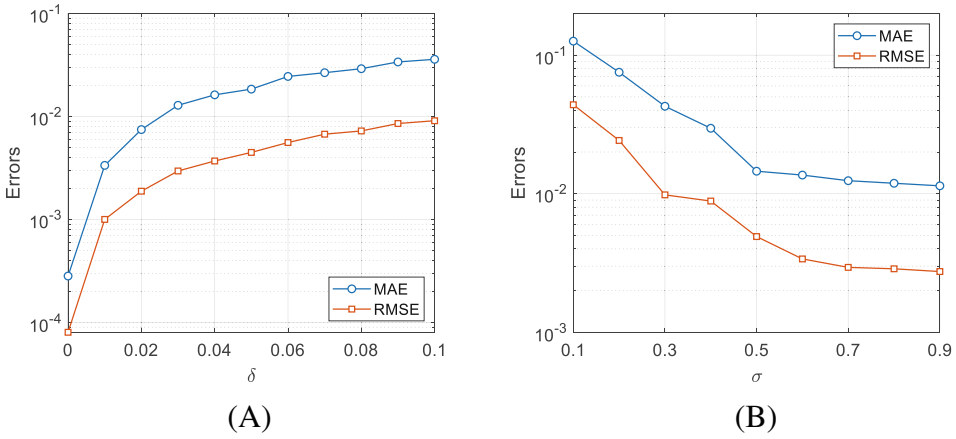

FIGURE 4 Convergence curves of the LKM with respect to (A) the noise level and (B) the percentage of the accessible boundary. In the investigation of the noise level, the percentage of the accessible boundary is fixed with (A) $\sigma = 75\%$. In the investigation of the noise level, the noise level is fixed with (B) $\delta = 3\%$

TABLE 2 The MAEs and RMSEs obtained by the LKM with various techniques of local approximation, under $\delta = 3\%$ and $\sigma = 75\%$

m	10	20	30	40	50	60	70	80
MAE	1.308*e*-02	1.209*e*-02	1.314*e*-02	1.132*e*-02	1.263*e*-02	1.158*e*-02	1.125*e*-02	1.156*e*-02
RMSE	3.370*e*-03	3.338*e*-03	3.151*e*-03	3.455*e*-03	3.490*e*-03	3.795*e*-03	3.719*e*-03	4.017*e*-03
CPU-time(s)	0.231	0.401	0.539	0.785	1.125	1.449	1.922	2.371

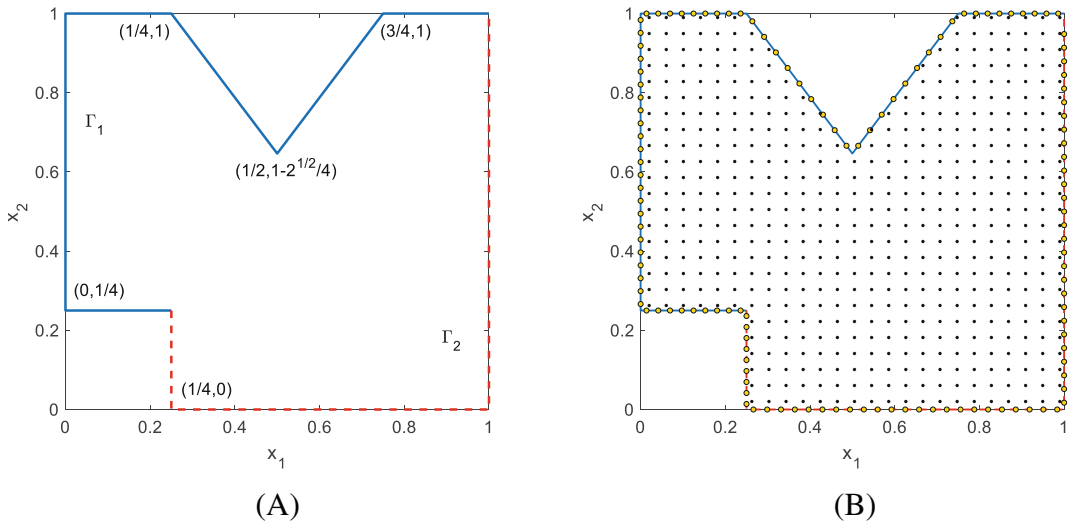

FIGURE 5 (A) Geometry configuration and (B) nodal distribution for example 2

It should be noticed that the use of a regularization method is normally required whenever attempting to solve stably an inverse problem. In order to investigate the accuracy of the proposed method in conjunction with regularization techniques, Figure 8 shows the predicted results on the inaccessible boundary obtained by using the LKM without and with regularization techniques in solving final system, when 3% noise is added to the known boundary data. In the calculation, four regularization methods (TSVD-LC, TSVD-GCV, Tikhonov-LC, Tikhonov-GCV) are introduced into the LKM for solving the resultant linear system (Equation 13). The performance of the algorithm uses the MATLAB functions in Hansen's regularization toolbox.[29] For more details of the regularization methods, we refer to References 30, 31. It

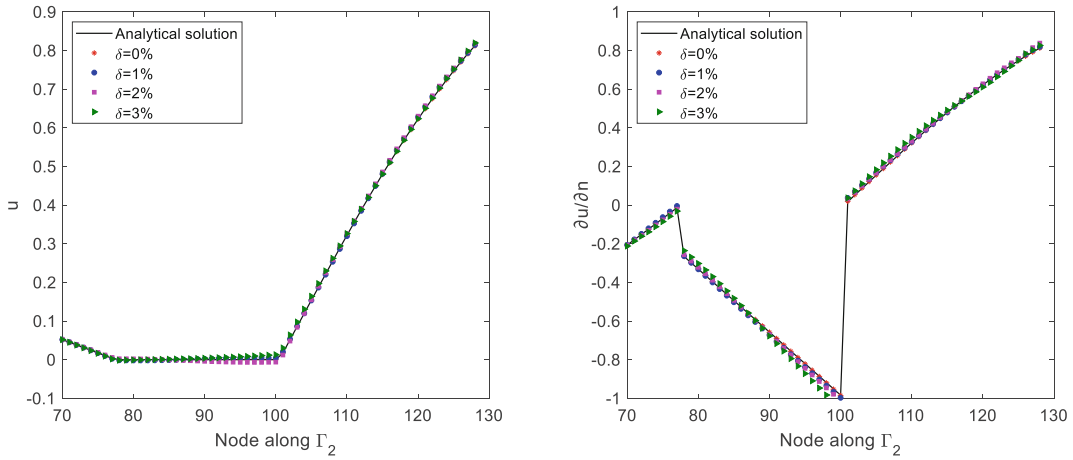

FIGURE 6 Reconstructed data on the inaccessible boundary under various noise levels. (A) Dirichlet boundary condition; (B) Neumann boundary condition

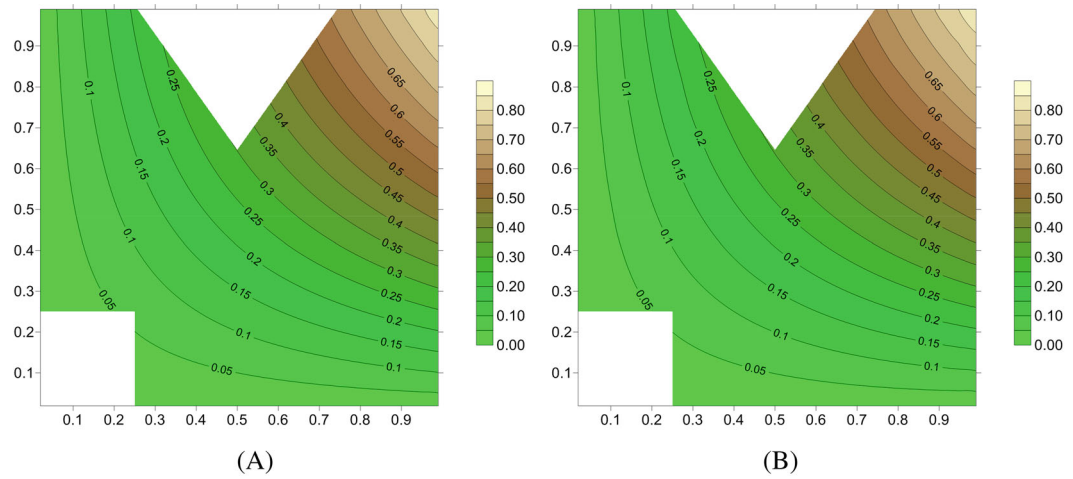

FIGURE 7 Comparison of (B) numerical and (A) analytical solutions on the computational domain under the noise level $\delta = 2\%$

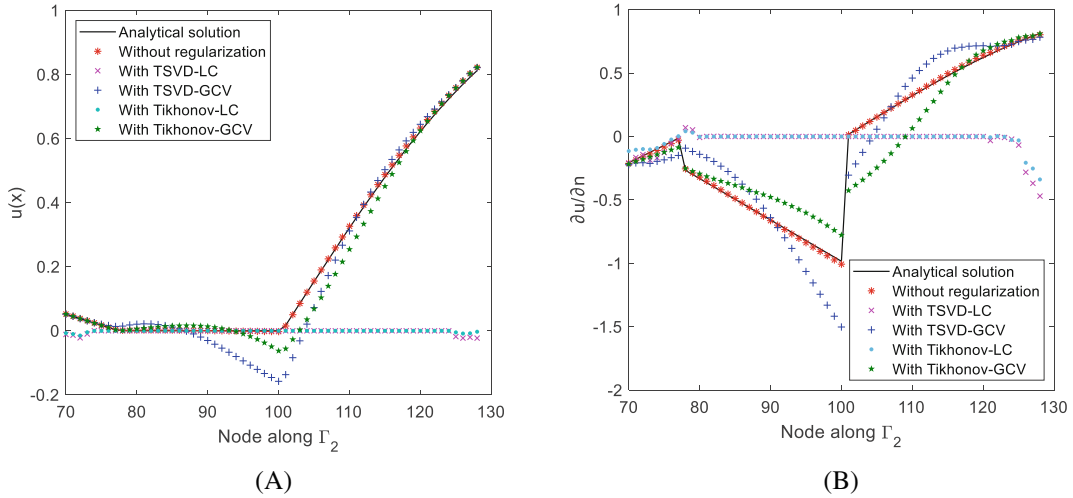

FIGURE 8 Reconstructed data on the inaccessible boundary obtained by using the LKM, when 3% noise is added to the known boundary data. (A) Dirichlet boundary condition; (B) Neumann boundary condition

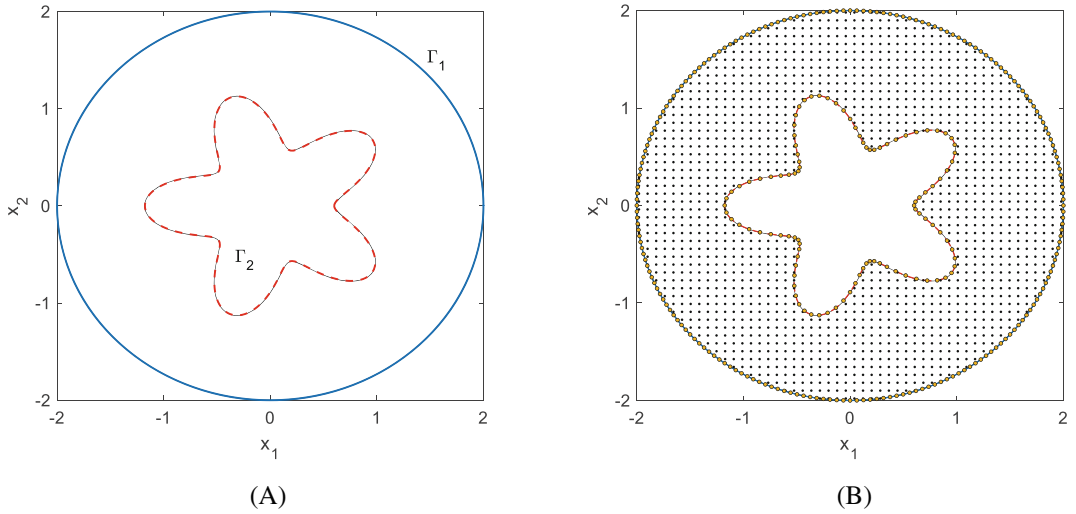

FIGURE 9 (A) Geometry configuration and (B) nodal distribution for example 3

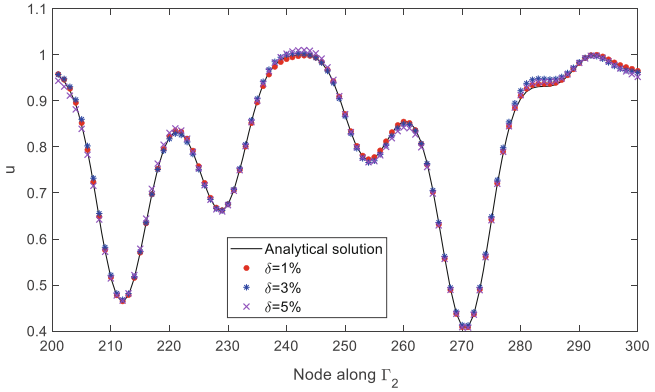

FIGURE 10 Reconstructed data on the inaccessible boundary with various noise levels

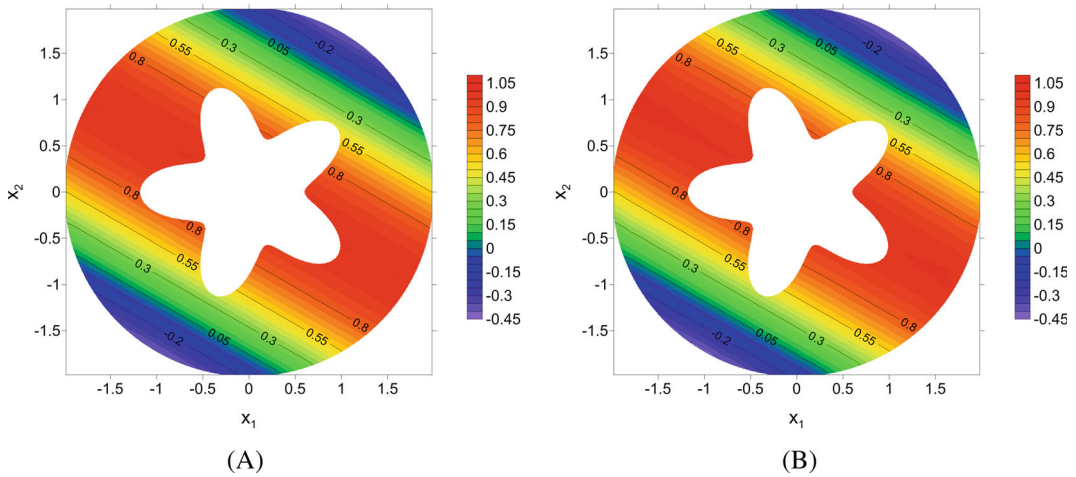

FIGURE 11 Comparison of numerical and analytical solution in the computational domain with $\delta = 3\%$ noise level. (A) Analytical solution; (B) LKM solution

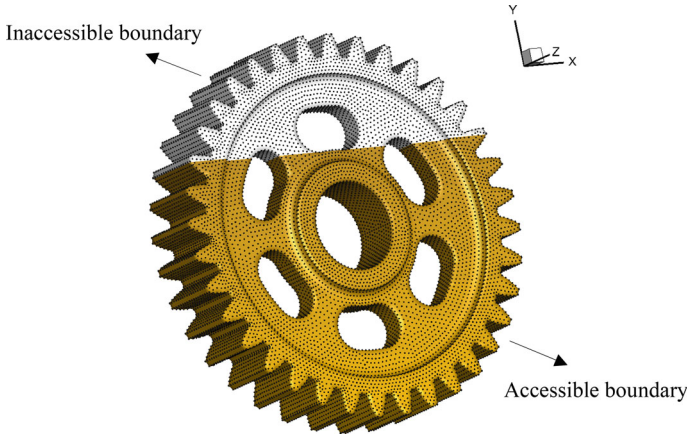

FIGURE 12 Geometry model and nodal distribution in Example 3

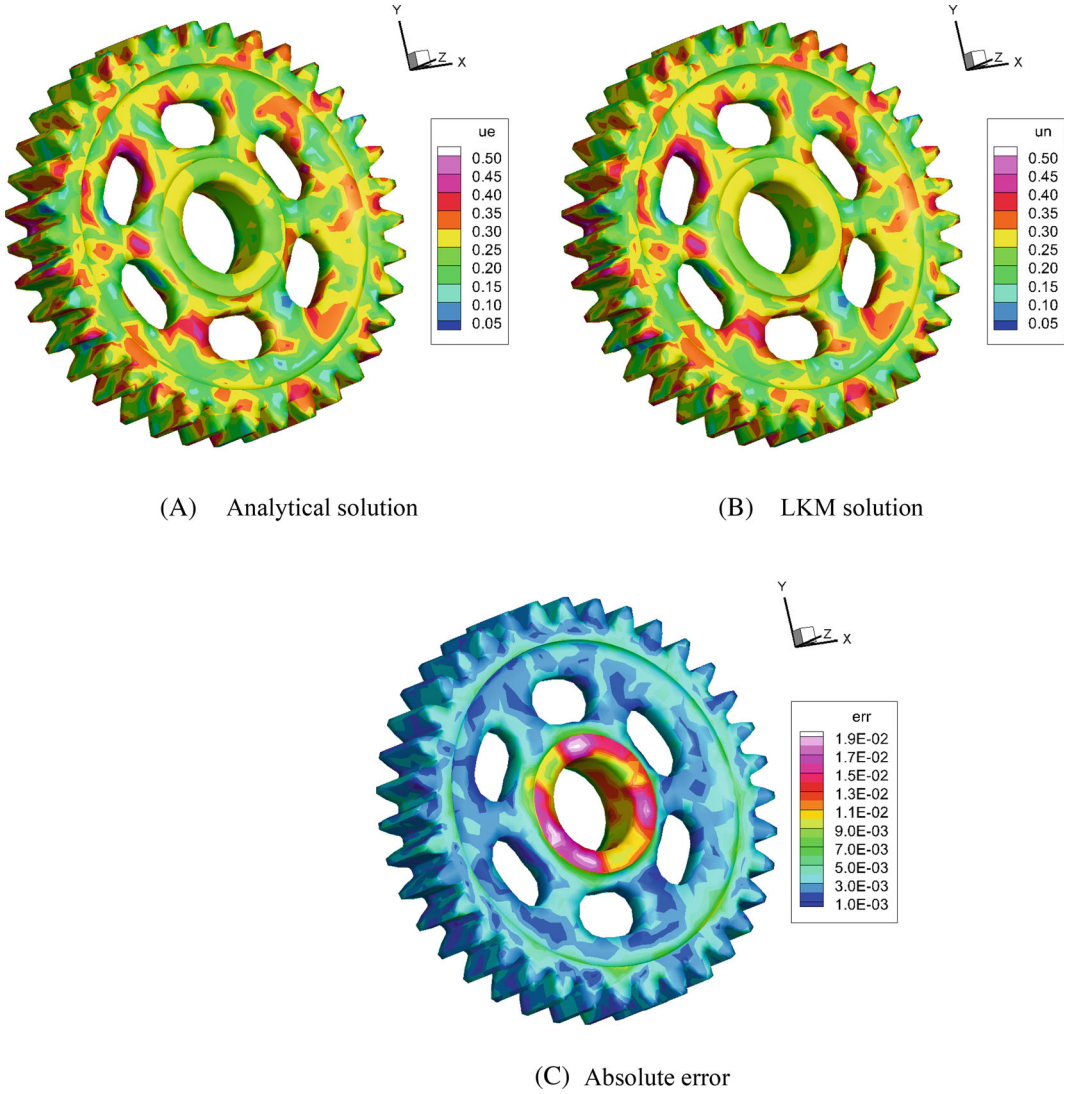

(A) Analytical solution (B) LKM solution

(C) Absolute error

FIGURE 13 Comparison of numerical results on the boundary under the noise level $\delta = 2\%$: (A) exact solution, (B) reconstruction solution, (C) absolute error

TABLE 3 The *RMSE*s of the LKM under different values of δ, σ, and m

$m = 50, \sigma = 70\%$		$m = 50, \delta = 2\%$		$\delta = 2\%, \sigma = 70\%$	
δ	RMSE	σ	RMSE	m	RMSE
0	1.417e-04	50%	6.960e-03	40	4.286e-03
1%	2.451e-03	60%	5.486e-03	50	4.356e-03
3%	5.812e-03	70%	4.356e-03	60	4.361e-03
5%	1.267e-02	80%	3.780e-03	70	3.470e-03

can be seen from Figure 8 that the LKM without regularization method has the highest accuracy among all the tested methods. The TSVD-LC and Tikhonov-LC are highly inaccurate. Although there is a certain agreement, the numerical results from the TSVD-GCV and Tikhonov-GCV show huge errors, and cannot be considered as the reasonable solutions. This investigation demonstrate that the proposed LKM is accurate and stable, and does not need any regularization technique in solving the final system. On the contrary, the introduction of the regularization technique greatly reduces the accuracy of the proposed method.

Example 3. This example considers a Helmholtz equation in a doubly connected domain (see Figure 9A). The analytical solution is $u(x_1, x_2) = \cos(ax_1 + bx_2)$,[11] where $k = 1$, $a = 0.5$, and $b = \sqrt{k^2 - a^2}$. Here, the outer boundary $\Gamma_1 = \left\{(x_1, x_2) \,|x_1^2 + x_2^2 = 2\right\}$ is specified as the accessible part, and the inner boundary $\Gamma_2 = \{(\rho\cos(\theta), \rho\sin(\theta)) \mid \rho = (111 - 36\cos(5\theta))/125, \;\; 0 \le \theta \le 2\pi\}$ is specified as the inaccessible one.

In the simulation, $N = 1830$ total nodes, including 200 and 100 outer and inner boundary nodes, are placed on the computational domain, as illustrated in Figure 9B. The number of supporting nodes is fixed as $m = 30$, Figure 10 compares the numerical solutions on the inner boundary under various noise levels. Noted that the inversion results are in good agreement with the exact solutions, and the predicted values converge to the analytical solution decreasing noise level.

In order to examine the effect of the reconstruction in the computational domain, Figure 11 shows the numerical and analytical solutions in the computational domain with 3% noise level. The predicted result shown a quite agreement with the analytical one. This example indicates that the proposed approach is of relatively high accuracy and numerical stability in addressing inverse Cauchy problems of Helmholtz equations in a doubly connected domain.

Example 4. The third example considers an inverse Cauchy problem of Helmholtz equation on a 3D gear-shaped domain shown in Figure 12. The size of model is 0.6 m × 0.6 m × 0.1 m. To test the proposed method, the analytical solution $u(x_1, x_2, x_3) = \sin(x_1)\cos(x_2)\cos(x_3)$ with $k = \sqrt{3}$ is used in this model.

Set $N = 12546$, $n_i = 2092$, $n_{b1} = 7318$, $n_{b2} = 3136$, $m = 50$, $\sigma = 70\%$, and $\delta = 2\%$, Figure 12 depicts the nodal distribution of the LKM, the accessible and inaccessible parts of the boundary. Figure 13 gives the comparison of analytical and reconstructed results on the surface, where the errors of LKM are $MAE = 1.987e-02$ and $RMSE = 4.356e-03$. The LKM solution is in good agreement with the analytical one, indicating to the accuracy and effectiveness of the proposed method.

To investigate the influence of parameters on the LKM, Table 3 lists the *RMSE*s under different values of δ, σ, and m. In the calculation, $N = 21153$ is fixed, the remaining parameters remain unchanged when one of the parameters is considered. It is obvious from Table 3 that the LKM converges with the decrease of noise level as well as the increase of accessible boundary. Moreover, various values of $40 \le m \le 70$ can guarantee reliable numerical results.

Example 4. The second example considers an inverse Cauchy problem of modified Helmholtz equation on a 3D car-shaped domain shown in Figure 14. The accessible part of the boundary and nodal distribution of the LKM are also plotted in Figure 14. The size of model is 1 m × 0.5 m × 2 m. In this investigation, we employ the analytical solution $u(x_1, x_2, x_3) = e^{\left(x_1 + x_2/2 + \sqrt{11}x_3/2\right)}$ with $k = 2$.

Under $N = 82840$, $n_i = 36412$, $n_{b1} = 27857$, $n_{b2} = 18571$, $m = 60$, $\sigma = 60\%$, and $\delta = 3\%$, numerical results of $u(\boldsymbol{x})$ and $\partial u(\boldsymbol{x})/\partial \boldsymbol{n}$ on the boundary are plotted in Figures 15 and 16, respectively. It can be observed that the present LKM can achieve an accurate and stable approximation of unknowns on the unmeasurable boundary, even for a relatively high noise level (3%) and a larger proportion of the inaccessible boundary (40%).

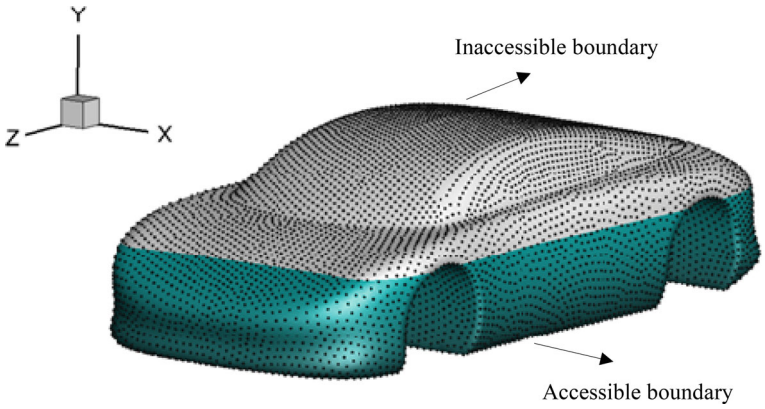

FIGURE 14 Geometry model and nodal distribution in Example 4

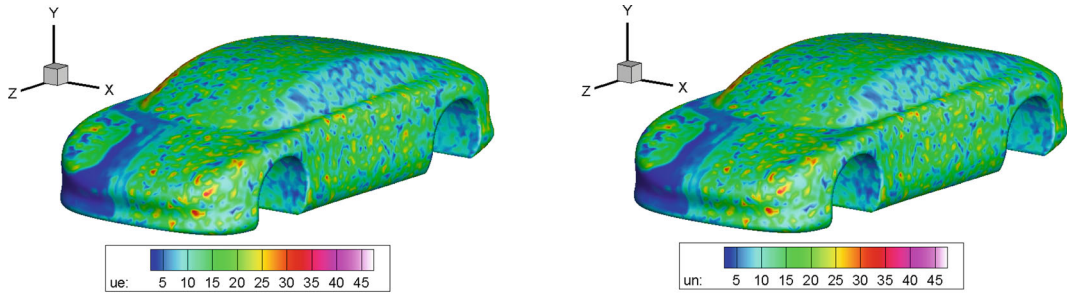

FIGURE 15 Comparison for analytical and numerical results of $u(\boldsymbol{x})$ on the boundary. (A) Analytical solution; (B) LKM solution

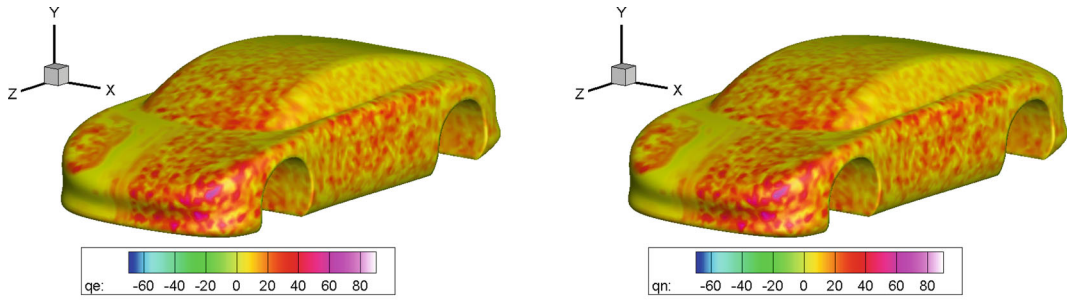

FIGURE 16 Comparison for analytical and numerical results of $\partial u(\boldsymbol{x})/\partial \boldsymbol{n}$ on the boundary. (A) Analytical solution; (B) LKM solution

The above numerical experiments with complicated geometries confirm the capacity and potential of the proposed methodology in solving the inverse Cauchy problems of Helmholtz equations on the high dimensional and complex domains.

6 | CONCLUSIONS

This study established a new meshless model for solving the inverse Cauchy problems of Helmholtz equations on arbitrary domains with the help of the LKM and the Moore–Penrose pseudoinverse. Numerical experiments including 3D

simply- and multi-connected domains shown the reconstruction results under various noise levels, and indicated the good performance of the new methodology. Compared with the existing methods, the proposed LKM formulation has the following merits.

1. The proposed approach uses the non-singular general solution satisfied governing equation, and captures the characteristics of semi-analytical and local approximation. Therefore, it can achieve an accurate and stable numerical result, and is suitable for the simulations of inverse problem with a large-scale and/or complicated geometry.
2. The proposed scheme uses the truncated singular value decomposition to obtained the Moore–Penrose inverse in the local approximation of supporting domain, and thus other regularization techniques are not needed in solving the resultant line system. The use of Moore–Penrose pseudoinverse guarantees a good behavior of local approximation system, which leads to a well-conditioned resultant system.
3. The inverse Cauchy problem of Helmholtz equations on 3D complicated domains is a difficult issue. The present method and program are easy to use in both 2D and 3D problems. Therefore, this study provides a novel, accurate and efficient tool for addressing the high dimensional and complex inverse problems associated with Helmholtz equations.

ACKNOWLEDGMENT

The work described in this article was supported by the National Natural Science Foundation of China (No. 11802151) and the Natural Science Foundation of Shandong Province of China (No. ZR2019BA008).

DATA AVAILABILITY STATEMENT

The data that support the findings of this study are available from the corresponding author upon reasonable request.

ORCID

Fajie Wang https://orcid.org/0000-0002-5162-1099
Yanpeng Gong https://orcid.org/0000-0002-3177-2826

REFERENCES

1. António J, Tadeu A, Godinho L. A three-dimensional acoustics model using the method of fundamental solutions. *Eng Anal Bound Elem*. 2008;32:525-531.
2. Tadeu A, António J, Godinho L. Defining an accurate MFS solution for 2.5D acoustic and elastic wave propagation. *Eng Anal Bound Elem*. 2009;33:1383-1395.
3. Kirkup S. The boundary element method in acoustics: a survey. *Appl Sci*. 2019;9:1642.
4. Tadeu A, António J, Castro I. Coupling the BEM/TBEM and the MFS for the numerical simulation of acoustic wave propagation. *Eng Anal Bound Elem*. 2010;34:405-416.
5. Tadeu A, Stanak P, Sladek J, Sladek V. Coupled BEM–MLPG acoustic analysis for non-homogeneous media. *Eng Anal Bound Elem*. 2014;44:161-169.
6. Regińska T, Regiński K. Approximate solution of a Cauchy problem for the Helmholtz equation. *Inverse Probl*. 2006;22:975-989.
7. Delvare F, Cimetière A, Pons F. An iterative boundary element method for Cauchy inverse problems. *Comput Mech*. 2002;28:291-302.
8. Fan C-M, Li P-W, Yeih W. Generalized finite difference method for solving two-dimensional inverse Cauchy problems. *Inverse Probl Sci Eng*. 2015;23:737-759.
9. Nachaoui A, Nachaoui M, Chakib A, Hilal M. Some novel numerical techniques for an inverse Cauchy problem. *J Comput Appl Math*. 2021;381:113030.
10. Marin L. Boundary element–minimal error method for the Cauchy problem associated with Helmholtz-type equations. *Comput Mech*. 2009;44:205-219.
11. Marin L, Lesnic D. The method of fundamental solutions for the Cauchy problem associated with two-dimensional Helmholtz-type equations. *Comput Struct*. 2005;83:267-278.
12. Marin L. An alternating iterative MFS algorithm for the Cauchy problem for the modified Helmholtz equation. *Comput Mech*. 2010;45:665-677.
13. Chen W, Fu Z-J. Boundary particle method for inverse Cauchy problems of inhomogeneous Helmholtz equations. *J Mar Sci Technol*. 2009;17:157-163.
14. Chan H-F, Fan C-M. The local radial basis function collocation method for solving two-dimensional inverse Cauchy problems. *Numer Heat Transf B Fund*. 2013;63:284-303.

15. Liu C-S, Qu W, Chen W, Lin J. A novel Trefftz method of the inverse Cauchy problem for 3D modified Helmholtz equation. *Inverse Probl Sci Eng*. 2017;25:1278-1298.
16. Jin B, Zheng Y. Boundary knot method for some inverse problems associated with the Helmholtz equation. *Int J Numer Methods Eng*. 2005;62:1636-1651.
17. Jin B, Zheng Y. Boundary knot method for the Cauchy problem associated with the inhomogeneous Helmholtz equation. *Eng Anal Bound Elem*. 2005;29:925-935.
18. Wang F, Chen W, Jiang X. Investigation of regularized techniques for boundary knot method. *Int J Numer Methods Biomed Eng*. 2010;26:1868-1877.
19. Sun L, Zhang C, Yu Y. A boundary knot method for 3D time harmonic elastic wave problems. *Appl Math Lett*. 2020;104:106210.
20. Wang F, Gu Y, Qu W, Zhang C. Localized boundary knot method and its application to large-scale acoustic problems. *Comput Methods Appl Mech Eng*. 2020;361:112729.
21. Yue X, Wang F, Zhang C, Zhang H. Localized boundary knot method for 3D inhomogeneous acoustic problems with complicated geometry. *App Math Model*. 2021;92:410-421.
22. Wang F, Wang C, Chen Z. Local knot method for 2D and 3D convection–diffusion–reaction equations in arbitrary domains. *Appl Math Lett*. 2020;105:106308.
23. Yue X, Wang F, Li P-W, Fan C-M. Local non-singular knot method for large-scale computation of acoustic problems in complicated geometries. *Comput Math Appl*. 2021;84:128-143.
24. Wang F, Fan C-M, Hua Q, Gu Y. Localized MFS for the inverse Cauchy problems of two-dimensional Laplace and biharmonic equations. *Appl Math Comput*. 2020;364:124658.
25. Qu W, Fan C-M, Gu Y, Wang F. Analysis of three-dimensional interior acoustic fields by using the localized method of fundamental solutions. *App Math Model*. 2019;76:122-132.
26. Wang F, Chen Z, Li P-W, Fan C-M. Localized singular boundary method for solving Laplace and Helmholtz equations in arbitrary 2D domains. *Eng Anal Bound Elem*. 2021;129:82-92.
27. Barata JCA, Hussein MS. The Moore–Penrose pseudoinverse: a tutorial review of the theory. *Braz J Phys*. 2012;42:146-165.
28. https://www.mathworks.com/help/matlab/ref/pinv.html.
29. Hansen PC. Regularization tools version 4.0 for Matlab 7.3. *Numer Algorithms*. 2007;46:189-194.
30. Wang F, Chen W, Gu Y. Boundary element analysis of inverse heat conduction problems in 2D thin-walled structures. *Int J Heat Mass Transfer*. 2015;91:1001-1009.
31. Wang F, Chen W, Qu W, Gu Y. A BEM formulation in conjunction with parametric equation approach for three-dimensional Cauchy problems of steady heat conduction. *Eng Anal Bound Elem*. 2016;63:1-14.

How to cite this article: Wang F, Chen Z, Gong Y. Local knot method for solving inverse Cauchy problems of Helmholtz equations on complicated two- and three-dimensional domains. *Int J Numer Methods Eng*. 2022;1-16. doi: 10.1002/nme.7061